Electrowetting Dynamics of Microfluidic Actuation

K.-L. Wang and T. B. Jones*

Department of Electrical and Computer Engineering, University of Rochester, Rochester, New York 14627

Received December 17, 2004. In Final Form: February 23, 2005

When voltage is suddenly applied to vertical, parallel dielectric-coated electrodes dipped into a liquid with finite conductivity, the liquid responds by rising up to reach a new hydrostatic equilibrium height. On the microfluidic scale, the dominating mechanism impeding this electromechanically induced actuation appears to be a dynamic friction force that is directly proportional to the velocity of the contact line moving along the solid surface. This mechanism has its origin in the molecular dynamics of the liquid coming into contact with the solid surface. A simple reduced-order model for the rising column of liquid is used to quantify the magnitude of this frictional effect by providing estimates for the contact line friction coefficient. Above some critical threshold of voltage, the electromechanical force is clamped, presumably by the same mechanism responsible for contact angle saturation and previously reported static height-of-rise limits. The important distinction for the dynamic case is that the onset of the saturation effect is delayed in time until the column has risen more than about halfway to its static equilibrium height.

Introduction

Essential to the operation of the laboratory-on-a-chip (LOC) and other micro-total analysis systems (μTASs) is some sort of microfluidic plumbing system to dispense, move, manipulate, and mix tiny volumes of liquid analyte and reagent. Taking many forms, electrically coupled schemes are favored because they have no moving parts and provide direct flow control. The two principal electrical mechanisms for manipulating liquids are *electroosmosis*, primarily for pumping liquid in closed-channel systems, and *electromechanical actuation*, more useful in open structures. Electromechanical schemes can be further differentiated as follows: (i) electrostatic droplet transport systems,[1−3] (ii) electrowetting-on-dielectric (EWOD) schemes,[4−6] and (iii) dielectrophoretic (DEP) liquid actuation.[7,8] Common to almost all are dielectrically coated electrodes and at least one free liquid surface contained by a nonuniform electric field. The speed and relatively simple geometries of open systems offer some distinct advantages in μTAS designs.

The volume of published papers indicates rapidly growing interest in electrowetting as a microfluidic mechanism. Industry-supported research and development of optical and fluidic switches,[9,10] low-cost electronic displays,[11] and tunable lenses[12,13] is in progress. Also, LOC-related applications for integrated biochemical reactors[14,15] and droplet dispensers[16] have been proposed. In many of these schemes, especially optical systems and displays, response time is crucial. Unfortunately, because insufficient attention has been directed to the dynamics of EWOD and DEP microactuation, performance optimization methodologies for them are primitive or lacking altogether. Part of the problem is that hydrodynamics on the microfluidic scale rearranges the relative importance of momentum, viscosity, gravity, capillarity, and surface wetting. In particular, the dynamic behavior of the moving contact line (also called the "three-phase line") between the conductive, working liquid, the solid substrate, and air (or an insulating host liquid) is not well understood.

In previous work, we clarified the relation between static EWOD and DEP microactuation with dielectric height-of-rise measurements on a modified Pellat fixture,[17] showing that these effects are respectively the low- and high-frequency limits of the electromechanical response of a dielectric liquid with finite conductivity. The subject of this paper is the dynamic behavior of liquids in the same experimental configuration and the same range of electric field magnitudes and frequencies. The parallel-plate Pellat geometry is a good choice for experimental investigations of electrowetting because of its simplicity and because it is very similar to certain microfluidic schemes.[5,6] Data obtained for aqueous solutions and ethylene glycol reveal when and how saturation influences the dynamics as a function of frequency and voltage. We present a reduced-order hydrodynamic model based on a control volume formulation for comparison to the experiments. This model and the data supporting it lead us to conclude that a contact line friction mechanism having

* Corresponding author. E-mail: jones@ece.rochester.edu.

(1) Washizu, M. *IEEE Trans. Ind. Appl.* **1998**, *34*, 732−737.
(2) Torkkeli, A.; Saarilahti, J.; Häärä, A.; Härmä, H.; Soukka, T.; Tolonen, P. *IEEE/MEMS Conf. Techn. Dig.* **2001**, 475−478.
(3) Vykoukal, J.; Schwartz, J. A.; Becker, F. B.; Gascoyne, P. R. C. *Micro Total Anal. Syst. Conf.* **2001**, 72−74.
(4) Welters, W. J. J.; Fokkink, L. G. J. *Langmuir* **1998**, *14*, 1535−1538.
(5) Lee, J.; Moon, H.; Fowler, J.; Schoellhammer, T.; Kim, C.-J. *Sens. Actuators, A* **2002**, *95*, 259−268.
(6) Pollack, M. G.; Fair, R. B.; Shenderov, A. *Appl. Phys. Lett.* **2000**, *77*, 1725−1726.
(7) Jones, T. B.; Gunji, M.; Washizu, M.; Feldman, M. *J. Appl. Phys.* **2001**, *89*, 1441−1448.
(8) Ahmed, R.; Hsu, D.; Bailey, C.; Jones, T. B. *Microscale Thermophys. Eng.* **2004**, *14*, 761−768.
(9) Cattaneo, F.; Baldwin, K.; Yang, S.; Krupenkin, T.; Ramachandran, S.; Rogers, J. A. *J. Microelectromech. Syst.* **2003**, *12*, 907−912.
(10) Huh, D.; Tkaczyk, A. H.; Bahng, J. H.; Chang, Y.; Wei, H.-H.; Grotberg, J. B.; Kim, C.-J.; Kurabayashi, K.; Takayama, S. *J. Am. Chem. Soc.* **2003**, *125*, 14678−14679.
(11) Hayes, R. A.; Feenstra, B. J. *Nature* **2003**, *425*, 383−385.
(12) Krupenkin, T.; Yang, S.; Mach, P. *Appl. Phys. Lett.* **2003**, *82*, 316−318.
(13) Kuiper, S.; Hendriks, B. H. *Appl. Phys. Lett.* **2004**, *85*, 1128−1130.
(14) Shen, Y.; Liu, Z.; Jacquot, B. C.; Minch, B. A.; Kan, E. C. *Sens. Actuators, B* **2004**, *102*, 35−43.
(15) Srinivasan, V.; Pamula, V. K.; Fair, R. B. *Lab Chip* **2004**, *4*, 310−315.
(16) Hoshino, K.; Triteyaprasert, S.; Matsumoto, K.; Shimoyama, I. *Sens. Actuators, A* **2004**, *114*, 473−477.
(17) Jones, T. B.; Wang, K.-L.; Yao, D.-J. *Langmuir* **2004**, *20*, 2813−2818.

10.1021/la0468702 CCC: $30.25
Published on Web 03/23/2005

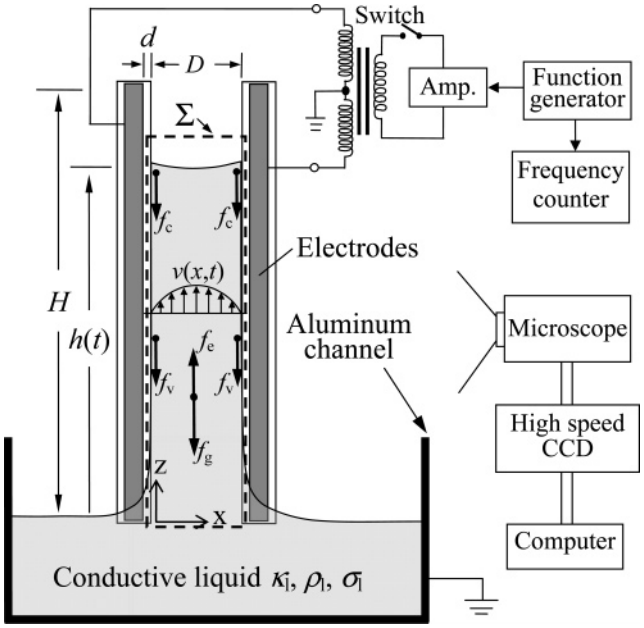

Figure 1. The modified Pellat's experiment uses two parallel, coated electrodes to actuate conductive liquid of dielectric constant κ_l, density ρ_l, and conductivity σ_l. Electrodes at spacing D are dipped <1 mm into liquid. Bipolar ac or dc is applied by a piezoelectric switch. The transient height of rise, $h(t)$, is recorded using a high-speed video camera attached to a stereomicroscope. A reduced-order hydrodynamic model, based on an assumed parabolic (Poiseuille) velocity profile, is formulated for the control volume enclosed by Σ, and with the gravitational, f_g, electrical, f_e, viscous shear, f_v, and contact line friction, f_c, forces acting on the liquid column rising between the electrodes.

its origin in liquid molecular dynamics dominates over viscous shear in impeding the flow. In addition, observations indicate a possible correlation between the transient contact line velocity and the time-varying contact angle of the moving meniscus.

Hydrodynamic Model

Figure 1 shows the parallel electrode structure with spacing D, width W, and vertical length H. The conditions $D \ll W \ll H$ ensure that the electric field between the two electrodes is uniform and that the fringing field can be neglected in the model. The spacing, D, is smaller than the static equilibrium height for experimental voltages ≥100 V-rms. The Reynolds number, Re, never exceeds ~4 for ethylene glycol and ~250 for the aqueous solutions. Therefore, we can make the further assumption of laminar flow with a 2D Poiseuille velocity profile.[18]

The rising liquid column is enclosed by the control volume, Σ, shown in Figure 1. Consistent with Huang et al.,[19] we assume a no-slip, Poiseuille velocity profile for the flow.

$$v_z(x,t) = v_0(t)\frac{4}{D^2}[x(D-x)] \tag{1}$$

where $v_0(t)$ is the maximum, time-dependent velocity at the centerline $x = D/2$. The average velocity, dh/dt, is defined to describe the net upward motion of the liquid.

$$\frac{dh}{dt} = \frac{1}{D}\int_0^D v_z(x,t)\,dx \tag{2}$$

Combining eqs 1 and 2 and integrating yields

$$\frac{dh}{dt} = 2v_0(t)/3 \tag{3}$$

The conservation of momentum for the fluid column in Σ is stated as

$$\frac{d}{dt}\left(\rho_l WDh\frac{dh}{dt}\right) = f_g + f_v + f_c + f_e \tag{4}$$

where

$$\rho_l WDh\frac{dh}{dt}$$

is the momentum of the rising column and ρ_l is the liquid density. The right-hand side of eq 4 consists of the gravitational force, f_g, the viscous force, f_v, due to shear stress at the walls, the contact line friction, f_c, associated with molecular kinetics and energy dissipation,[20] and the driving electrical force, f_e, which is suddenly applied at $t = 0$. The gravitational force on the mass is

$$f_g = -\rho_l gWDh \tag{5}$$

A general expression for the viscous drag forces is

$$f_v = -2Wh\tau_z \tag{6}$$

where τ_z is the shear stress, which is linearly related to the flow velocity and proportional to the liquid viscosity, μ_l. Using the velocity profile, eq 1

$$\tau_z = \mu_l\frac{\partial v_z}{\partial x} = \frac{6\mu_l}{D}\frac{dh}{dt} \tag{7}$$

The contact line frictional force, f_c, depends on the contact line velocity, dh/dt,[21,22]

$$f_c = -2\xi W\frac{dh}{dt} \tag{8}$$

where ξ is the contact line friction coefficient in newton-seconds per square meter. Equation 8 is actually an approximation of Blake and Haynes's original theory[20] deemed valid for the velocity range of the experiments reported.

The driving force of electrical origin, f_e, which can be obtained using the Maxwell stress tensor derived from the Korteweg–Helmholtz body force density,[23,24] is

$$f_e = \rho_l gWDK^*(\omega)V^2u(t) \tag{9}$$

where $K^*(\omega)$ is a frequency-dependent coefficient,[17] V is the rms voltage, and $u(t)$ is the unit step function.

(18) Young, D. F.; Munson, B. R.; Okiishi, T. H. *A brief introduction to fluid mechanics*; Wiley: Toronto, 1997; Chapters 6 and 8.
(19) Huang, W.; Bhullar, R. S.; Fung, Y. C. *J. Biomech.* **2001**, *123*, 446–454.
(20) Blake, T. D.; Haynes, J. M. *J. Colloid Interface Sci.* **1969**, *30*, 421–423.
(21) Decamps, C.; De Coninck, J. *Langmuir* **2000**, *16*, 10150–10153.
(22) Ren, H.; Fair, R. B.; Pollack, M. G.; Shaughnessy, E. J. *Sens. Actuators, B* **2002**, *87*, 201–206.
(23) Jones, T. B. *Langmuir* **2002**, *18*, 4437–4443.
(24) Jones, T. B.; Fowler, J. D.; Chang, Y. S.; Kim, C.-J. *Langmuir* **2003**, *19*, 7646–7651.

$$K^*(\omega) = \frac{\epsilon_0\kappa_d{}^2[\epsilon_0{}^2\omega^2(\kappa_l - 1)(\kappa_l d + \kappa_d D/2) + \sigma_l{}^2 d]}{4\rho_l g(2d + \kappa_d D)[\epsilon_0{}^2\omega^2(\kappa_l d + \kappa_d D/2)^2 + \sigma_l{}^2 d^2]} \quad (10)$$

κ_l and σ_l are the relative permittivity and conductivity of the liquid, respectively, κ_d and d are the relative permittivity and thickness of the dielectric layer, respectively, $\epsilon_0 = 8.854 \times 10^{-12}$ F/m, and $g = 9.81$ m/s^2. Equation 10 is based on the assumption that $d \ll D$.

Equations 5−10 combine to give the time-dependent equation of motion.

$$\frac{d}{dt}\left[h\frac{dh}{dt}\right] + \frac{12\mu}{\rho D^2}h\frac{dh}{dt} + \frac{2\xi}{\rho D}\frac{dh}{dt} = g[K^*(\omega)V^2 - h], \quad t \geq 0 \quad (11)$$

with initial conditions $h|_{t=0} = 0$ and $(dh/dt)|_{t=0} = 0$. Note that the steady-state limit is $h|_{t\to\infty} = h_s = K^*V^2$. Before proceeding with the solution of eq 11, it is useful to compare the laminar viscous and dynamic contact line friction terms.

$$F_c = \frac{12\mu|h|\left|\frac{dh}{dt}\right|/\rho D^2}{2\xi\left|\frac{dh}{dt}\right|/\rho D} = \frac{6\mu|h|}{\xi D} \quad (12)$$

By setting $F_c = 1$ and using the static, low-frequency limit for $|h|$, that is, $K^*(\omega\to 0)V^2 = \kappa_d\epsilon_0 V^2/4\rho g d D$, we can identify a critical voltage, V^*, denoting the boundary between the viscous and contact line force limited regimes.

$$V^* = \sqrt{\frac{2\xi\rho g d D}{3\mu\kappa_d\epsilon_0}} \quad (13)$$

For $V \ll V^*$, contact line friction dominates, while, for $V \gg V^*$, viscosity is more important. Decamps and De Coninck measured the dynamic spreading of glycerol droplets on crystalline PTFE and estimated $\xi = 4.4$ (N s)/m^2.[21] Using this value and parameters typical for ethylene glycol experiments yields $V^* \sim 1.4 \times 10^4$ V-rms, which is considerably higher than the values used in our experiments. Thus, we conclude that dynamic contact line friction dominates over laminar viscous drag.

Introducing a new variable, $y = h^2$, simplifies eq 11 to a form more convenient for solution using MATLAB.

$$\frac{d^2y}{dt^2} + \left(\frac{12\mu}{\rho D^2} + \frac{2\xi}{\rho D\sqrt{y}}\right)\frac{dy}{dt} + 2g\sqrt{y} = 2gK^*(\omega)V^2 \quad (14)$$

Figure 2 plots numerical solutions of eq 11 for deionized (DI) water with $\xi = 0$ and 0.5 (N s)/m^2. Note that, for $\xi = 0$ (the solid line), the column is predicted to overshoot and exhibit damped oscillation about the static equilibrium position, h_s, presumably due to momentum gained by the column as it rises. On the other hand, no overshoot is predicted for $\xi = 0.5$. Furthermore, with ξ set to this value, laminar viscous drag seems to have no influence on the transient dynamics for viscosity $\mu = 0.9 \times 10^{-3}$ (N s)/m^2, the accepted value for water at laboratory ambient temperature. Therefore, at least at the lower voltages, the contact line friction is predicted to dominate over viscous drag and to determine the characteristic time of the transient motion of the column.

Experiment

Setup. The apparatus shown in Figure 1 is virtually identical to that used in earlier, static height-of-rise experiments.[17] Two parallel electrodes, made of 60 × 12 × 1.5 mm^3 polished stainless steel plates, were coated with $d = 3.5 \pm 0.5$ μm parylene of dielectric constant $\kappa_d = 3.1$. No surface treatment was used, but prior to each experiment, the coated electrodes were wiped with Midel 7131, a halogen-free pentaerythritol ester oil. The properties of this oil are summarized in Table 1. A very thin film, of a thickness estimated by ellipsometry to be less than ~1 μm, significantly abates wetting stiction and contact angle hysteresis with a negligible effect on the effective dielectric thickness. Once the oil is applied to the electrodes, many experiments can be conducted, yielding highly reproducible data. The electrodes were carefully positioned in a U-shaped aluminum channel with glass side walls and immersed no more than 1 mm into the liquid to minimize parasitic capacitance and any consequent imbalance in the voltage distribution between the electrodes.

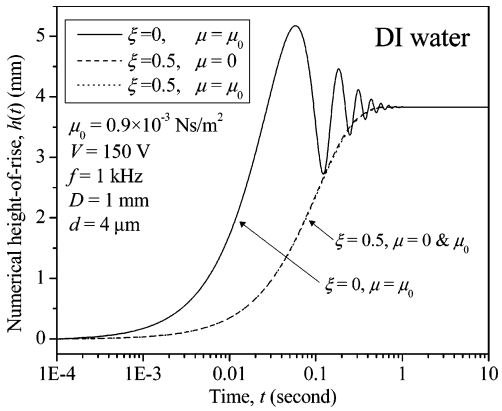

Figure 2. Numerical height of rise calculated from eq 11 plotted versus time. In this calculation, the ac voltage is 150 V-rms at 1 kHz, the DI water is of viscosity $\mu_0 = 0.9 \times 10^{-3}$ (N s)/m^2, and the electrode spacing and dielectric thickness are $D = 1$ mm and $d = 4$ μm, respectively. With the contact line friction coefficient $\xi = 0.5$ (N s)/m^2, the $h(t)$ curves for both $\mu = 0$ (dashed line) and μ_0 (dotted line) completely overlap and tend to the static equilibrium value, h_s, for $t \geq 0.4$ s. On the other hand, the viscous-only model ($\mu = \mu_0$ and $\xi = 0$, solid line) predicts significant overshoot and damped oscillation of the rising column as it settles to the static limit. In the experiments, overshoot is not observed for $D = 1$ mm.

Most experiments were performed using bipolar alternating current (ac) voltage from 50 Hz to 5 kHz, which was supplied by a pair of identical, series-connected, step-up transformers driven by a power amplifier. See Figure 1. In all experiments, the liquid was grounded through the metallic channel containing it. With voltage application controlled by a piezoelectric switch, the rise time achieved was <0.1 ms, much shorter than the liquid mechanical response time. Alternating current (ac) voltage magnitudes and frequencies were measured with a true-rms multimeter (Fluke model no. 87) and an electronic counter (Fluke model no. 1900A).

Dynamic height-of-rise data were obtained from individual video frames taken by a high-speed CCD camera (Photron Fastcam-PCI) coupled to a stereomicroscope (Zeiss Stemi SV6) and operated at frame rates up to 1000 fps. Table 1 shows the properties of the four experimental liquids.

Phenomenology. The sequence of video clips in Figure 3 captures typical, dynamic behavior for DI water at 2 kHz and 700 V-rms. The electrode spacing, $D \sim 1.8$ mm, somewhat larger than the values typically used for data gathering, permitted observation of the meniscus and the contact angle during the upward motion of the liquid column. Due to the moderate hydrophobicity of the oil-treated parylene layer, the liquid makes a contact angle with the parylene of 80−85° before the voltage is switched on at $t = 0$ (Figure 3a). When the voltage is applied, the curvature of the meniscus increases very rapidly without a visible change in the height; within ~2 ms, the contact angle decreases to ~60° (Figure 3b). This change occurs on a time scale short compared to the rise of the liquid column. Upward motion becomes evident at ~3 ms, and the curvature actually decreases starting at ~4 ms, as shown in Figure 3c. In the following few tenths of a second, the column moves rapidly upward while the contact angle increases slightly (Figure 3d and e). In this

Table 1. Experimental Liquid Properties at 24 °C

liquid	Midel 7131	DI water	0.1 M mannitol	0.8 M mannitol	ethylene glycol
conductivity, σ_l [a] (mS/m)	$<10^{-7}$	0.15 ± 0.05	0.35 ± 0.05	0.45 ± 0.05	0.055 ± 0.005
dynamic viscosity[b] ($\mu_0 = 0.9 \times 10^{-3}$ (N s)/m^2)	$\sim 78\mu_0$	μ_0	$\sim 1.08\mu_0$	$\sim 1.2\mu_0$	$\sim 16.5\mu_0$
relative permittivity, κ_l	3.2	80	~80	~80	37.7
density, ρ_l (10^3 kg/m^3)	0.97	1	1.02	1.145	1.11

[a] Measured with a YSI model no. 35 conductance meter. [b] Measured with a Brookfield model no. DV-I digital viscometer.

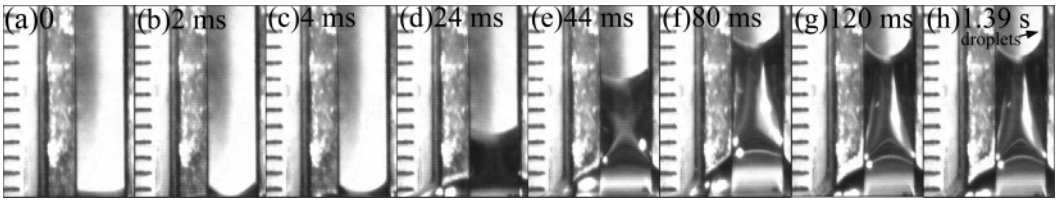

Figure 3. Selected images clipped from video recorded at 1000 fps showing the transient behavior of DI water between two electrodes spaced at ~1.8 mm at 2 kHz and 700 V-rms. At $t = 0_-$ (voltage off), the meniscus has a contact angle of $\theta_c \sim 80-85°$ (a). When voltage is applied, the contact angle decreases to 60° within 2 ms (b) and the curvature of the meniscus increases without any noticeable rise of the liquid. When the liquid starts rising at ~4 ms, the contact angle increases somewhat and the meniscus flattens (c). The column now rises rapidly to 3−4 mm, while θ_c remains roughly constant at ~60° (d and e). The column overshoots the static limit, h_s, reaches a maximum height at ~80 ms (f), and then recedes, leaving $\theta_c \sim 55°$ due to contact angle hysteresis (g). The liquid column then exhibits damped oscillations and finally settles to the static limit after ~1 s (h). The arrow points out tiny droplets that often form on the electrodes just above the contact line.

particular experiment, the column reaches a maximum height at ~80 ms (Figure 3f) and then recedes, leaving the contact angle at 55° (Figure 3g), possibly due to contact angle hysteresis. The overshoot is consistent with simulations performed for large electrode spacings, as shown in Figure 2. After several oscillations (~1 s), the meniscus settles to the static limit, h_s, and tiny droplets are often observed to form along the contact line (Figure 3h).

The same experiment performed with water at similarly large spacings but lower frequencies (<200 Hz) reveals a vigorous, side-to-side sloshing motion of the liquid surface as it rises. This electrohydrodynamic surface wave phenomenon is probably parametric in nature and may have a strong influence on the transient motion for $D \geq 1.5$ mm.

Results

Most dynamic height-of-rise data were obtained at a spacing of $D = 0.7 \pm 0.05$ mm, where curvature-related error is negligible, overshoot is not observed, and no liquid sloshing is evident. For convenience in observation, the height, h, was measured from the liquid level outside the electrodes to the lowest point of the meniscus. This choice, while arbitrary, introduces minimal error because, except right after the voltage is turned on, the height of rise is large compared to the observed radius of curvature.

Frequency Dependence. Figure 4 shows the time-dependent height of rise of DI water for $D = 0.7 \pm 0.05$ mm at 125 V-rms with dc and ac voltages from 100 Hz to 5 kHz. At any particular frequency, the column rises 3.5−5 mm within ~0.2 s, approaching a steady value identical to the static height, h_s, measured by slowly increasing the voltage. This height of rise is larger at low frequencies and decreases dramatically above 2 kHz, just as with the static experiments, where the transition from EWOD to DEP occurs.[17] Plotted solutions of eq 11 match the time course of the data very well if a mean squared error minimization method is used to identify the best-fit values for ξ. Refer to the Appendix. In the initial stages of the transient motion, that is, $t < 0.01$ s, measured height values are somewhat lower than predictions, due to limits on measurement precision or possibly because the model does not account for entrance effects.

Effect of Viscosity. Figure 5 plots height-of-rise data for DI water, two aqueous mannitol solutions, and ethylene glycol at fixed voltage and frequency. As in Figure 4, the continuous curves are solutions to eq 11 using best-fit

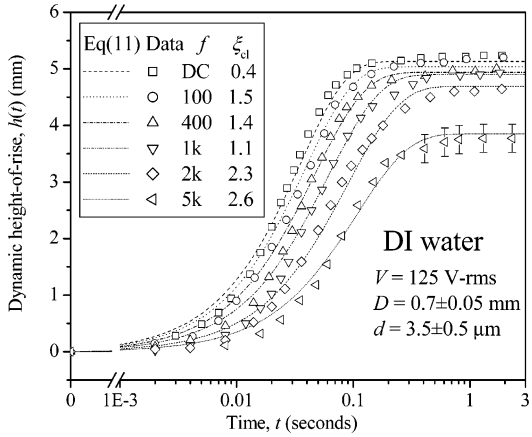

Figure 4. Frequency dependence of the height of rise, $h(t)$, versus time, t, for DI water at 125 V-rms and frequencies ranging from dc to 5 kHz ac. For clarity, only about half the data are included. The plotted curves are solutions to eq 11 based on values of the dynamic contact line friction coefficient, ξ, that minimize the mean squared error (mse) using the method described in the Appendix. At very short times (<20 ms), the model overestimates $h(t)$, possibly because of the measurement errors shown by a few representative error bars. Another factor may be entrance effects not included in the model.

values for ξ obtained by the method described in the Appendix. DI water and the aqueous mannitol solutions have fairly similar mechanical responses and are closely fitted by values of ξ ranging from 0.52 to 0.94 (N s)/m^2. Ethylene glycol, which is far more viscous, responds more slowly. The best-fit coefficient, $\xi = 4.75$ (N s)/m^2, is roughly a factor of 10 greater than the value for DI water. Perhaps only coincidentally, this value is comparable to the value 4.4 (N s)/m^2 obtained by Decamps and De Coninck for glycerol droplets spreading under the influence of an electric field on dry PTFE-coated electrodes.[21]

Voltage Dependence and Saturation. The dynamic data in Figures 4 and 5 are closely matched by numerical solutions of eq 11 with properly fitted ξ values; however, above some voltage threshold, this agreement deteriorates. We find that this threshold is strongly correlated to the saturation phenomenon observed in static height-of-rise experiments.[17] Figure 6 plots height of rise versus time for ethylene glycol at a spacing of $D = 0.7 \pm 0.05$ mm and

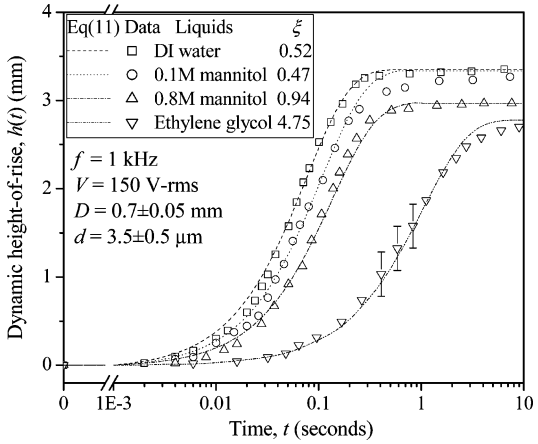

Figure 5. Plots of $h(t)$ vs t for aqueous solutions and ethylene glycol showing a strong correlation of transient motion to liquid viscosity. The curves are solutions to eq 11 based on values of the dynamic contact line friction coefficient, ξ, that minimize the mean squared error (mse) using the method described in the Appendix. For DI water and the mannitol solutions, with a dynamic viscosity of $\mu \sim 10^{-3}$ (N s)/m^2, the best-fit ξ values are quite similar. On the other hand, ethylene glycol is ~16 times more viscous and ξ is about an order of magnitude higher than the aqueous media.

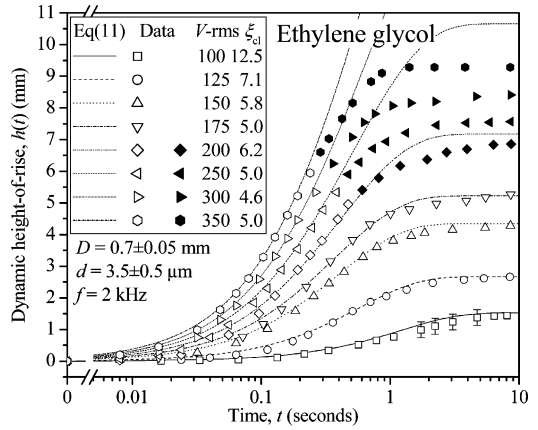

Figure 6. Voltage dependence of the height of rise, $h(t)$, vs time, t, for ethylene glycol. For $V \leq 175$ V-rms, the data closely follow the voltage-square law, but, for $V \geq 200$ V-rms, dynamic saturation (indicated by solid symbols) is observed as the column approaches the static limit. All coefficient values, ξ, are obtained by mean squared error minimization using transient data indicated by the open symbols. For $V \leq 175$ V-rms, all the data can be used, whereas, for $\geq$200 V-rms, only data before the saturation onset are employed. Refer to the Appendix for an explanation of how the saturation onset is identified.

voltages from 100 to 350 V-rms. For $V \leq 175$ V-rms, all data follow the predicted voltage-square relationship and are consistent with the numerical solutions throughout the entire time course of the transient motion. On the other hand, for $V \geq 200$ V-rms, only an initial portion of the transient data can be fitted successfully by the model. In Figure 6, the open symbols signify data used to obtain the values for ξ obtained via mean squared error minimization. The solid symbols represent data not included in the curve fitting. The Appendix shows that the mean squared error starts to rise dramatically if these data points are used.

At some point in time during the transient motion, the liquid column undergoes an abrupt deceleration, suggesting that the electromechanical force has been clamped. The most reasonable explanation for this clamping is a delayed but sudden onset *in time* of the same mechanism responsible for (i) contact angle saturation and (ii) the clamping force observed in static, height-of-rise[4,17] and excess pressure[24] measurements. There is no consensus about what causes saturation, but perhaps its delayed onset when the contact line is moving will provide some clues as to its physical origin.

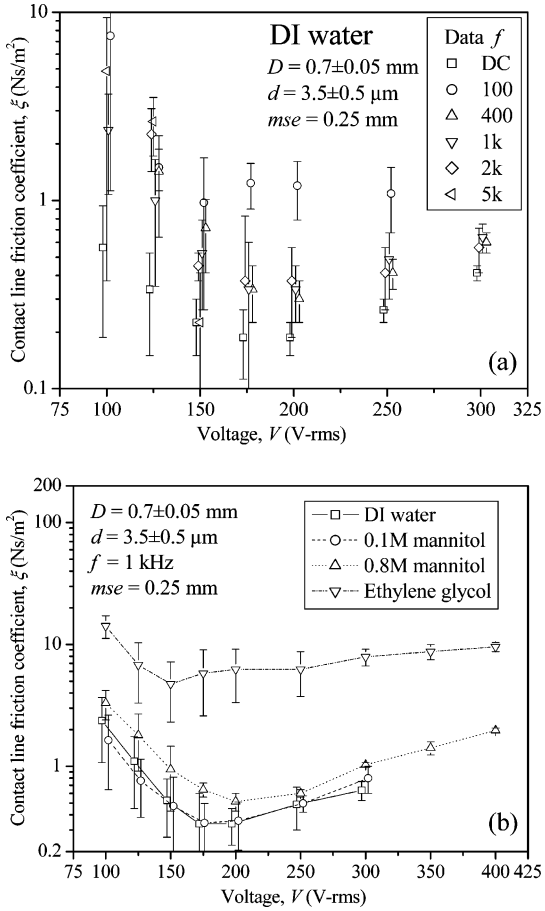

Figure 7. Contact line friction coefficients, ξ, extracted by mean squared error minimization plotted versus voltage. For $V < 150$ V-rms, the data scatter is large because of measurement precision limits, and the larger values of ξ may be due to entrance effects not included in the model. (a) ξ vs V for DI water at a frequency from dc to ac 5 kHz. (b) Plots for several liquids showing strong correlation of ξ to viscosity, μ. For clarity, some data have been slightly shifted along the abscissa.

Frequency and Voltage Dependence of ξ. Figure 7a plots ξ values from mean squared error minimization versus voltage for DI water at frequencies ranging from dc to 5 kHz ac. For $V \geq 175$ V-rms, ξ is not strongly dependent upon voltage. It must be remembered that these values are obtained using only data points *before* the onset of saturation. The considerable scatter for $V < 125$ V-rms is probably caused by measurement errors when $h(t)$ is small. Entrance effects may also play a role. Another possible explanation is that, for the experiments conducted at lower voltages, the liquid surface remains close to the fringing field in violation of the uniform field approximation upon which eq 9, the electromechanical force, is based. All the factors mentioned tend to overestimate the electrical driving force and, in consequence, to overestimate ξ. Figure 7b plots ξ values for DI water, 0.1 and 0.8 M mannitol solutions, and ethylene glycol.

Figure 8 shows that, for the liquids tested, there is at best a rather weak dependence of the contact line coefficient on frequency from dc to 5 kHz. These data reflect the previously noted correlation of ξ to liquid viscosity, μ. This correlation might be explained at a fundamental level

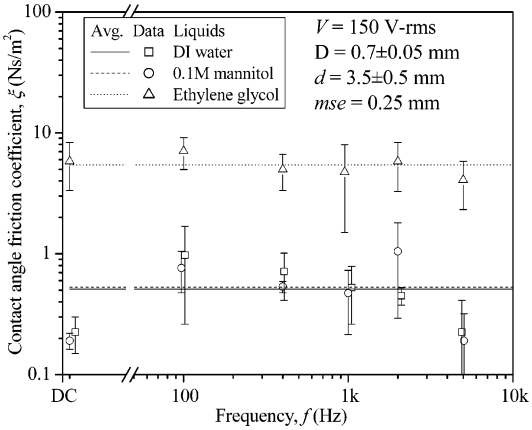

Figure 8. Plots of the coefficient ξ versus frequency for ethylene glycol and aqueous liquids showing at best modest dependence from dc up to 5 kHz. Note that the average value for ethylene glycol, $\xi = 5.5$ (N s)/m^2, is an order of magnitude higher than the value for aqueous solutions, $\xi = 0.55$ (N s)/m^2.

by referring to the common molecular dynamical origin of both contact line friction[20] and viscous momentum transfer.

Discussion

Justification of the fully developed Poiseuille velocity profile, that is, eq 1, involves tests of two independent criteria. First, because the flow is transient, the development of a steady velocity profile depends on the relative values of the viscous diffusion time, $\tau_v = \rho_l D^2/\mu_l$, and the transient, mechanical time, τ_m, required for the column to rise to its equilibrium position. If $\tau_v \ll \tau_m$, then, at the very least, eq 1 provides a good description of the profile in the middle portion of the column far from the entrance region and the moving meniscus. For ethylene glycol, $\tau_v = 0.03$ s and $\tau_m \geq 0.3$ s, confirming that the velocity profile in the moving column is well-developed for this liquid. On the other hand, for DI water, $\tau_v = 0.42$ s and $\tau_m \geq 0.03$ s, indicating that the Poiseuille velocity profile assumption is not justified, at least for higher voltages.

The second criterion involves comparing the lengths of the entrance region at the bottom and the transition region at the top near the meniscus to the total column height, h. Huang et al. argue that the two length scales are comparable,[19] so we here concentrate on the lower, entrance region. For these transient flows, the maximum Reynolds numbers are estimated to be ~4 and ~250 for ethylene glycol and aqueous solutions, respectively. However, more realistic values can be obtained using average, measured velocities of 20 and 100 mm/s, respectively. These numbers yield values for the flow that we deem more representative, namely, $Re \sim 1$ and $Re \sim 75$, once again, respectively. The entrance length at the bottom of the electrodes can be estimated from $l_e = 0.06ReD$.[18] Using this equation with the above average Reynolds number values, we obtain $l_e \sim 0.05$ mm for ethylene glycol, much less than the static height of rise, and ~3 mm for aqueous liquids, which is comparable to the static height of rise, h_s, for applied voltages less than ~150 V-rms. Therefore, entrance effects are of consequence only for aqueous solutions, and then only at lower voltages. At the same time, concern about errors incurred in the viscous drag term in eq 11 for the rising liquid column for the case of water is largely allayed by the evidence that contact line friction completely dominates over the viscous drag for all liquids.

Effect of Oil Film. The Midel oil film on the parylene-coated electrodes is very effective in eliminating the slip−stick motion commonly observed in electrowetting-induced dynamics upon dielectric-coated electrodes. The reason for this improvement is not understood. The oil, applied with a moistened cloth and then rubbed vigorously, is very thin, probably less than 1 μm. We see no evidence that the water film displaces this film during voltage application; highly repeatable data can be obtained with an oil-treated electrode structure without any need for reapplication. A question arises concerning the true nature of the three-phase line. Can the oil-treated parylene be regarded as an effectively solid surface? One may object that our experimental "system" does not mimic dry surfaces used in many previous electrowetting investigations. Further, the oil film might influence the saturation phenomena. On the other hand, the success of the Midel oil-treated parylene suggests a new class of inexpensive, low-stiction surfaces having practical significance for EWOD-based microfluidic devices.

Contact Angle Observations. The captured video frames of Figure 3 reveal how the meniscus curvature and the contact angle evolve in time. In particular, the rapid decrease of the contact angle within 2 ms after the voltage is turned on (before the column starts to move) occurs on a time scale much shorter than the viscous diffusion time, τ_v. Typically, the liquid achieves its maximum velocity after ~3 ms and, starting at this time scale, contact line resistance dominates in limiting the flow. Accurate measurement of the contact angle of the moving meniscus requires better optical resolution than the video camera available to us provides. However, such measurements may facilitate a correlation of dynamic contact angle to height of rise, $h(t)$, and thereby elucidate the force clamping reported here.

Conclusion

We have used vertically oriented, parallel electrodes coated with parylene to investigate the transient, dynamic motion of slightly conductive liquids when voltage is applied suddenly. Liquids covering a range of viscosities were tested, including DI water, 0.1 and 0.8 M mannitol solutions, and ethylene glycol. A high-speed video camera was used to capture the upward transient motion and to reveal the time-dependent behavior of the contact angle and meniscus. For a suddenly applied electric field at small electrode spacings, the column rises upward, opposed by gravity, viscosity, and contact line friction, and asymptotically approaches the static limit. At large spacings, aqueous liquids, being less viscous, manifest overshoot and damped oscillatory behavior.

A reduced-order hydrodynamic model derived from the application of momentum conservation to a control volume and based on fully developed Poiseuille flow accurately predicts the transient motion of the rising column. Calculations of the entrance length and the viscous diffusion time show that this assumption is well justified in most experimental circumstances, except at the lowest voltages with aqueous liquids. The model incorporates the contact line friction mechanism first proposed by Blake and Haynes.[20] Both order-of-magnitude calculations and analysis of the data indicate that contact line friction completely dominates viscous drag at all test voltages. Supporting this contention is the good fit of numerical solutions of eq 11 using ξ, the contact line friction coefficient, as the single adjustable parameter to data obtained for several liquids over a range of voltages and frequencies.

Below the voltage-dependent threshold for contact angle saturation, the experimental data conform very well to

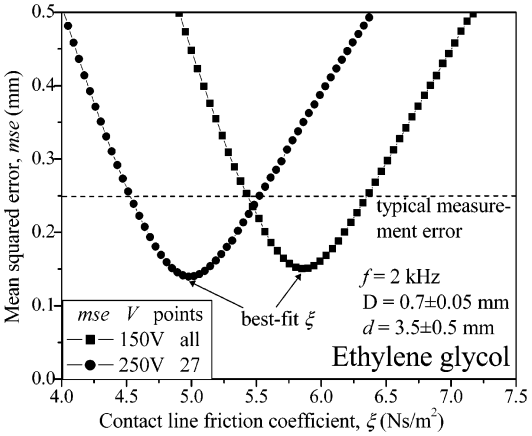

Figure 9. Dependence of the mean squared error (mse) upon trial values of the contact line friction coefficient, ξ, for ethylene glycol at 2 kHz using data from Figure 6. All experimental data at $V = 150$ V-rms are used to calculate the mse values, but only nonsaturation data (open symbols) are used for 250 V-rms data. The data in Figure 6 marked by solid symbols were excluded. The best-fit values, $\xi = 5.0$ and 5.8 (N s)/m^2, are obtained when mse = 0.14 and 0.15 mm, respectively. To identify the minima accurately, the scanning step size for ξ was set to 0.05 (N s)/m^2.

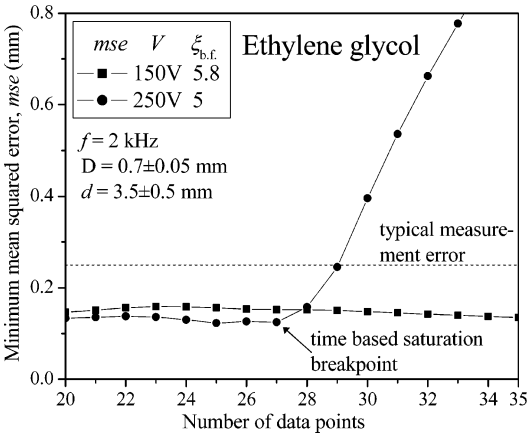

Figure 10. Plots of the mse calculated using eq A1 versus the number of experimental data points for data shown in Figure 6, based upon the best-fit coefficient values, ξ_{bf}. At $V = 150$ V-rms, which is below the saturation threshold, the mse remains constant as more points are added. On the other hand, at $V = 250$ V-rms, above the saturation threshold, addition of the 28th data point, corresponding to $t \sim 0.4$ s, heralds a rapid increase in the mse.

the voltage-square law and the frequency dependencies first reported for static measurements.[17,24] With contact line friction coefficient values, ξ, extracted using a mean squared error minimization method, excellent agreement of the predictive model to the experimental data results. The best-fit values of ξ are strongly correlated to liquid viscosity and rather weakly dependent upon voltage and frequency. When the voltage exceeds the saturation threshold, where one expects the electromechanical force to become clamped, the effect does not manifest itself immediately when the voltage is first applied. Instead, the force clamping occurs after the column has moved upward more than halfway to its final static equilibrium position at $h(t) = h_s$ and has already started to slow. The same mean square error method is again employed to extract estimates for the coefficient ξ using a truncated data set that extends from $t = 0$ up to the onset of saturation. This onset is clearly pinpointed by a rapid increase in the mean squared error if data points after saturation are included. We believe that the abrupt deceleration of the column occurs due to the same mechanism responsible for contact angle saturation. The explanation of why saturation is delayed in the dynamic Pellat experiment awaits the emergence of a well-supported model for the effect.

Acknowledgment. We are pleased to acknowledge Paul Osborne, who fabricated the test fixture, A. Raisanen at Rochester Institute of Technology, who helped with parylene coatings, and M&I Materials, Ltd., for providing the Midel oil used in the experiments. NIH, NSF, and the Infotonics Technology Center, Inc., supported this research.

Appendix

All best-fit values for the dynamic contact line friction coefficient, ξ, reported in this paper are obtained by minimizing the mean squared error between numerical solutions to eq 11 and individual sets of experimental data. The procedure involves calculation of the mean squared error (mse)

$$\text{mse} = \sqrt{\sum_{i}^{m} [h(t_i) - h_d(t_i)]^2 / m} \qquad \text{(A1)}$$

for trial values of the coefficient ξ and a search for the value that minimizes the mse. In eq A1, $h(t)$ and $h_d(t_i)$ are respectively numerical solutions of eq 11 and the experimental data values measured at m discrete times. Figure 9, plotting mse versus trial values of ξ for ethylene glycol at two voltages and 2 kHz, shows distinct minima. The best-fit value of ξ is assumed to correspond to $(\text{mse})_{\min}$, which we note is always smaller than the measurement precision.

For voltages below the saturation threshold, all experimental data points are used in eq A1 to calculate the mse and thence to estimate ξ via the minimization technique. In the saturation regime, the procedure is modified by identifying and using only data points before the occurrence of the abrupt deceleration. As indicated by Figure 6, the onset of saturation cannot be ascertained from visual examination of $h_d(t_i)$ data; however, mse minimization pinpoints it readily. Starting with a subset of data from $t = 0$ to $\sim$0.1 s, we use mean squared error minimization to estimate ξ. Then, adding one data point at time to the data set, we re-estimate ξ until $(\text{mse})_{\min}$ starts to increase. Figure 10 shows typical results obtained from this procedure. At $V = 150$ V-rms, $(\text{mse})_{\min}$ remains virtually constant as points are added, indicating that saturation never occurred and that the entire transient data set can be used for the ξ estimate. On the other hand, at $V = 250$ V-rms, $(\text{mse})_{\min}$ starts to rise rapidly when the 28th data point (corresponding to $t \sim 0.4$ s) is included, indicating abrupt deceleration of the column. We hypothesize a correspondence of this deceleration to clamping of the electrical force. Figure 9 teaches that the method produces a well-defined minimum for the mse, as long as saturation affected data are not incorporated in the estimate for ξ.

LA0468702